High-Velocity Magnetic Domain Wall Motion Driven by Acoustic Spin Transfer Torque

Jiacheng Lu[1], Fa Chen[1], Yiming Shu[1], Yukang Wen[1], Hang Zou[1], Yuhao Liu[1], Shiheng Liang[2], Wei Luo[1*], and Yue Zhang[1,3*]

[1]*School of Integrated Circuits, Huazhong University of Science and Technology, Wuhan 430074, China*
[2]*School of Physics, Hubei University, Wuhan 430062, China*
[3]*Songshan Lake Materials Laboratory, Dongguan 523808, China*

(Received 26 March 2025; accepted manuscript online 6 May 2025)

We predict high-velocity magnetic domain wall (DW) motion driven by out-of-plane acoustic spin in surface acoustic waves (SAWs). We demonstrate that the SAW propagating at a 30-degree angle relative to the x-axis of a 128° Y-$LiNbO_3$ substrate exhibits uniform out-of-plane spin angular momentum. This acoustic spin triggers the DW motion at a velocity exceeding 50 m/s in a way that is similar to the spin-transfer-torque effect. This phenomenon highlights the potential of acoustic spin in enabling rapid DW displacement, offering an innovative approach to developing energy-efficient spintronic devices.

DOI: 10.1088/0256-307X/42/6/067403 CSTR: 32039.14.0256-307X.42.6.067403

Surface acoustic waves (SAWs) and their magnetoacoustic interactions, particularly through magnetoelastic coupling, have emerged as a pivotal research frontier in magnetoelastic phenomena.[1–9] By inducing strain in magnetic materials, SAWs influence magnetization dynamics, paving the way for novel applications in low-dissipation spintronic and acoustic devices.

In recent years, significant progress has been made in utilizing SAWs to manipulate magnetic domain walls (DWs) through magnetoelastic coupling.[10–14] However, the velocity of DW motion induced by conventional SAWs, such as Rayleigh-type SAW, has been limited to around 1 m/s.[12] Simultaneously, advancements in understanding the angular momentum properties of acoustic waves have opened new possibilities for enhancing magnetoacoustic interactions. Traditionally characterized by their linear momentum, acoustic waves are now recognized for their intrinsic angular momentum, particularly spin angular momentum.[15–17] This has sparked growing interest in harnessing the spin angular momentum of SAWs to control magnetic moments, providing novel mechanisms for manipulating magnetic dynamics.

Our prior experimental work has revealed that when SAWs propagate at a 30-degree angle relative to the x-axis of a 128° Y-$LiNbO_3$ substrate, out-of-plane spin angular momentum emerges, which gives rise to nonreciprocal magnetoacoustic waves resulting from the breaking of crystal inversion symmetry.[18] In this work, we propose that this out-of-plane acoustic spin could induce the DW motion at a velocity higher than 50 m/s in a way similar to the spin-transfer-torque (STT) effect, marking a potential advancement for energy-efficient spintronic devices driven by SAWs.

We consider the model composed of the interdigitated transducers on the surface of lithium niobate (128° Y-$LiNbO_3$) with the orientation forming an angle with respect to the x-axis crystal axis of $LiNbO_3$ [Fig. 1(a)]. Using finite-element COMSOL Multiphysics® simulations, we characterized the strain components of SAWs at a central frequency of 1.04 GHz under 30 dBm input power, which is experimentally feasible. We found that when this angle is set to 30 degrees (we name it 30-degree SAW), the strain components of the SAW are composed of ε_{xx}, ε_{xy}, ε_{xz}, ε_{yz}, and ε_{zz}. Here, ε_{xx}, ε_{xz}, ε_{yz}, and ε_{zz} consist of the Rayleigh SAW, which, as will be confirmed below, does not contribute to the fast DW motion. Nevertheless, the ε_{xx} and ε_{xy} components [Fig. 1(b)] can generate acoustic wave spin ($\boldsymbol{S_z}$) along the out-of-plane orientation of the film, and the effective magnetoelastic field of this acoustic spin drives the Bloch-type DW [Fig. 1(c)] into rapid motion.

The simulated strain components for the 30-degree SAW are mainly composed of ε_{xx} and ε_{xy} as $\varepsilon_{xx} = Ak\sin(\omega t - kx)$ and $\varepsilon_{xy} = \frac{1}{2}Ak\sin(\omega t - kx + \pi/2)$. Here A, k, and ω are the displacement amplitude, the wavenumber, and the angular frequency of the SAW. Based on $\varepsilon_{xx} = \frac{\partial u_x}{\partial x}$, $\varepsilon_{xy} = \frac{1}{2}(\frac{\partial u_y}{\partial x} + \frac{\partial u_x}{\partial y})$, and $\boldsymbol{v} = \mathrm{d}\boldsymbol{u}/\mathrm{d}t$, the displacement $\boldsymbol{u}$ and the velocity field $\boldsymbol{v}$ are expressed as $\boldsymbol{u} = [A\cos(kx - \omega t),\ A\cos(kx - \omega t - \pi/2),\ 0]$ and $\boldsymbol{v} = [A\omega\cos(kx - \omega t - \pi/2),\ A\omega\cos(kx - \omega t - \pi),\ 0]$. The acoustic spin density $\boldsymbol{s}$ can be computed from the expression[19]

$$\boldsymbol{s} = \rho(\boldsymbol{u} \times \boldsymbol{v}). \tag{1}$$

The acoustic spin density of the 30-degree SAW was $\boldsymbol{s} = -A^2\omega\rho\boldsymbol{e}_z$. It exhibits a uniform spin density, with the spin

*Corresponding author. Email: luowei@hust.edu.cn; yue-zhang@hust.edu.cn
© 2025 Chinese Physical Society and IOP Publishing Ltd. All rights, including for text and data mining, AI training, and similar technologies, are reserved.

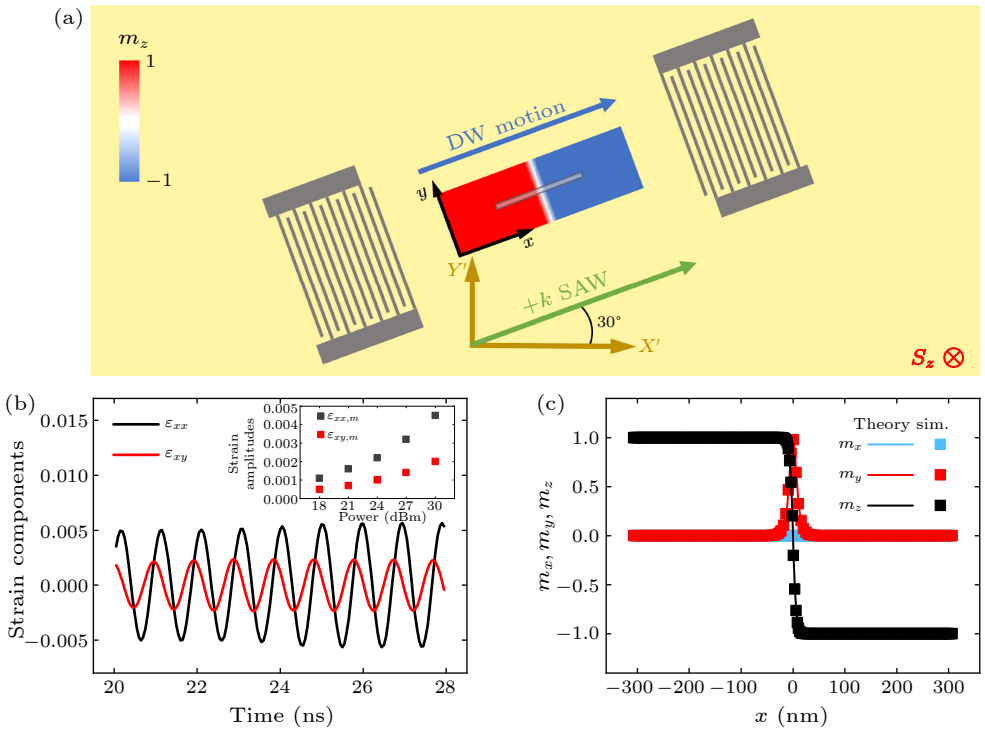

Fig. 1. (a) Schematic for the excitation of the SAW propagating at a 30-degree angle relative to the x-axis of a 128° Y-LiNbO$_3$ substrate and the driving of DW by this SAW. (b) Simulated ε_{xx} and ε_{xy} components of the strain for the 30-degree SAW at a frequency of 1.04 GHz (inset: the variation of the amplitudes of ε_{xx} and ε_{xy} of the 30-degree SAW under different excitation powers). (c) Walker profile of the Bloch DW in the magnetic film with perpendicular magnetic anisotropy, i.e., the magnetization distribution within the gray frame in (a).

polarization aligned along the out-of-plane direction of the magnetic film. The acoustic wave spin, in this context, refers to the rotation of the local velocity field of particles.[17] For the 30-degree SAW, all particles undergo coherent rotation within the xy plane, resulting in a uniform spin angular momentum. In addition to that, the SAW also carries orbital angular momentum, which, however, does not contribute significantly to the fast DW motion [S1 in the Supplementary Materials (SM)].

First, we discuss the physical mechanism for the influence of the SAW spin on the DW motion. Based on the relationship between the SAW spin and the ε_{xx} and ε_{xy} strain components, we have found that the magnetoelastic energy density $F_{\rm me} = b(\varepsilon_{xx}m_x^2 + 2\varepsilon_{xy}m_x m_y)$ can be converted to $F_{\rm me} = -\mu_0 \boldsymbol{H}_{\rm me}\cdot\boldsymbol{m}$, where the effective magnetoelastic field satisfies (S2 in the SM)

$$\boldsymbol{H}_{\rm me} = \frac{|b|k^2}{\mu_0 M_{\rm s}\varepsilon_{\rm m}\omega\rho}\eta \boldsymbol{R}(\zeta)\cdot(\boldsymbol{s}\times\boldsymbol{m}). \tag{2}$$

Here $\varepsilon_{\rm m}$ represents the strain amplitude of SAW. In Eq. (2), $\eta = \sqrt{\frac{3}{2} - \frac{\cos(2\omega t)}{2} + 2\sin(C)\sin(\omega t)}$ is the factor depicting that the strength of the magnetoelastic field oscillates around an average value $\langle H_{\rm me}\rangle_t = \sqrt{\frac{3}{2}}\frac{|b|\varepsilon_{\rm m}\sin\theta}{\mu_0 M_{\rm s}}$, where C is defined as $C = \omega t + 2\phi$, with ϕ representing the in-plane magnetization azimuth angle.

$$\boldsymbol{R}(\zeta) = \begin{bmatrix} \cos\zeta & -\sin\zeta & 0 \\ \sin\zeta & \cos\zeta & 0 \\ 0 & 0 & 1 \end{bmatrix}$$

with

$$\zeta = \frac{\pi}{2} - \arccos\left[\frac{-b[\sin(\omega t) + \sin C]}{|b|\sqrt{\frac{3}{2} - \frac{\cos(2\omega t)}{2} + 2\sin C\sin(\omega t)}}\right],$$

which indicates the counterclockwise rotation of the magnetoelastic field from $\boldsymbol{s}\times\boldsymbol{m}$ by an angle ζ, which oscillates around the average value $\bar{\zeta} = \frac{\pi}{2} - \arccos[-\sqrt{\frac{2}{3}}\frac{b\sin C}{|b|}]$. The following calculation will show that the oscillations of $\boldsymbol{H}_{\rm me}$ and ζ lead to weak fluctuations on the trajectory of the DW magnetization at the DW center. Therefore, we only considered the average magnetoelastic field expressed as

$$\langle \boldsymbol{H}_{\rm me}\rangle_T = \sqrt{\frac{3}{2}}\frac{|b|k^2}{\mu_0 M_{\rm s}\varepsilon_{\rm m}\omega\rho}\boldsymbol{R}(\bar{\zeta})\cdot(\boldsymbol{s}\times\boldsymbol{m}). \tag{3}$$

The $\boldsymbol{H}_{\rm me}$ can be decomposed into two components that are parallel and perpendicular ($\boldsymbol{H}_\perp$) to the magnetization, as illustrated in Fig. 2(a). The dynamics of the magnetization in the DW is determined by the torque of $\boldsymbol{H}_\perp$ acting on the magnetization, which is usually expressed as $\boldsymbol{\tau}_1 = \boldsymbol{m}\times\boldsymbol{H}_\perp$ and $\boldsymbol{\tau}_2 = \boldsymbol{m}\times(\boldsymbol{m}\times\boldsymbol{H}_\perp)$. Based on Eq. (3), it can be concluded that $\boldsymbol{\tau}_1 \sim \boldsymbol{m}\times(\boldsymbol{s}\times\boldsymbol{m})$ and $\boldsymbol{\tau}_2 \sim \boldsymbol{s}\times\boldsymbol{m}$, which are the same as the damping-like (DL) and field-like (FL) torques for the STT generated by an out-of-plane spin, respectively.

Unlike the STT for the spin of electrons, the DL and FL torques of acoustic spin have the same strength since they share the same coefficient in Eq. (3). Therefore, the coexistence of both torques drags the rotation of magnetization towards the acoustic spin along the z axis, which

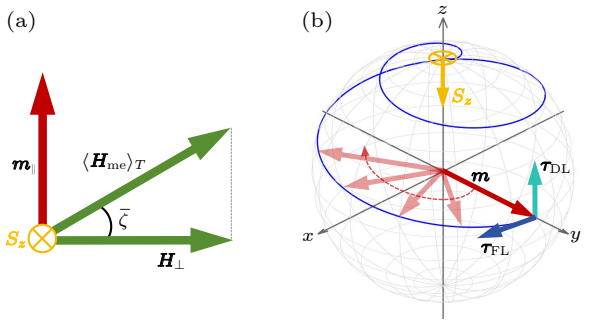

Fig. 2. (a) Schematic of the SAW spin, the average magnetoelastic field, and the xy-plane component of magnetization in the center of DW. (b) Schematic of the magnetization rotation in the center of DW (the red arrow) driven by the field-like (FL) and damping-like (DL) torque of the 30-degree SAW spin (the yellow arrow).

is accompanied by continuous magnetization precession in the xy plane, as illustrated in Fig. 2(b). This process sequentially happens for all the magnetization within the DW plane, resulting in the unidirectional DW motion accompanied by continuous magnetization rotation at the DW center.

To verify the above assumption, we simulated the DW motion by using the MUMAX3 simulation with the code of magnetoelastic interaction based on the parameters for perpendicularly magnetized Pt/Co and the $LiNbO_3$ substrate:[20] Gilbert damping coefficient $\alpha = 0.3$, gyromagnetic ratio $\gamma = 1.76 \times 10^{11}$ rad/T·s, vacuum permeability $\mu_0 = 4\pi \times 10^{-7}$ H/m, saturation magnetization $M_s = 5.8 \times 10^5$ A/m, exchange stiffness constant $A_{ex} = 1.5 \times 10^{-11}$ J/m, uniaxial anisotropy constant $K_u = 6 \times 10^5$ J/m^3, the velocity of SAW $v_{SAW} = 4000$ m/s, magnetoelastic coupling coefficient $b_1 = b_2 = -15.75 \times 10^6$ J/m^3, and density of Co $\rho = 8900$ kg/m^3.

As shown in Fig. 3(a), the strain field drives continuous DW displacement over 500 nm within a 10 ns duration, corresponding to an average velocity exceeding 50 m/s. In contrast, both the Rayleigh and shear-horizontal (SH) waves only result in weak oscillation, showing nearly no net displacement [inset of Fig. 3(a)]. The influence of the polarization direction of the SAW spin on DW motion is exhibited in Fig. 3(b). When the SAW propagates along the positive (negative) x-axis direction, it possesses spin angular momentum along the negative (positive) z-axis direction, driving the DW along the positive (negative) x-axis direction at a velocity of 49.98 m/s (52.80 m/s).

Figure 4 presents the relationship between DW motion and the acoustic wave frequency (f). In Fig. 4(a), the DW velocity initially increased with frequency, reaching a maximum value at approximately 0.88 GHz, above which it decreases sharply. This indicates the existence of a threshold frequency (f_{th}) for driving the DW. The inset in Fig. 4(b) illustrates the precession of magnetization in the DW center at frequencies lower and higher than f_{th}, and the phase-locking (phase-unlocking) precession occurred when $f < (>) f_{th}$. It is noteworthy that under the phase-unlocked condition, the DW displacement exhibits periodic oscillatory behavior. Our theoretical analysis will

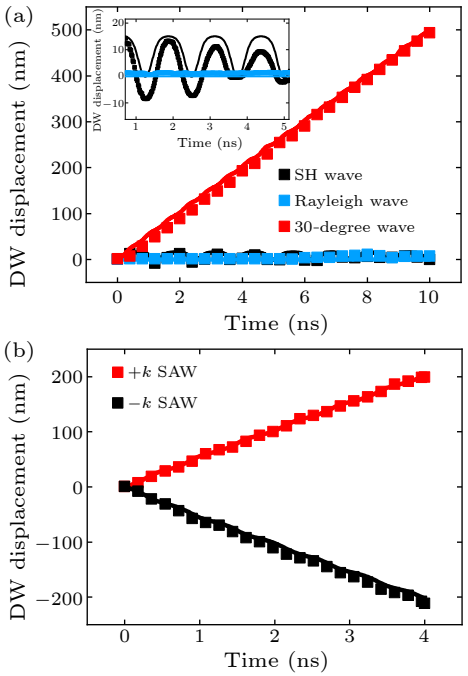

Fig. 3. (a) Comparison of the DW displacement driven by 30-degree SAW, Rayleigh SAW, and SH SAW at 0.8 GHz frequency (inset: enlarged portion for the DW motion driven by the Rayleigh SAW and SH SAW). (b) DW displacements under forward and backward propagation of the 30-degree SAW. The solid lines represent the calculated results of the CCM.

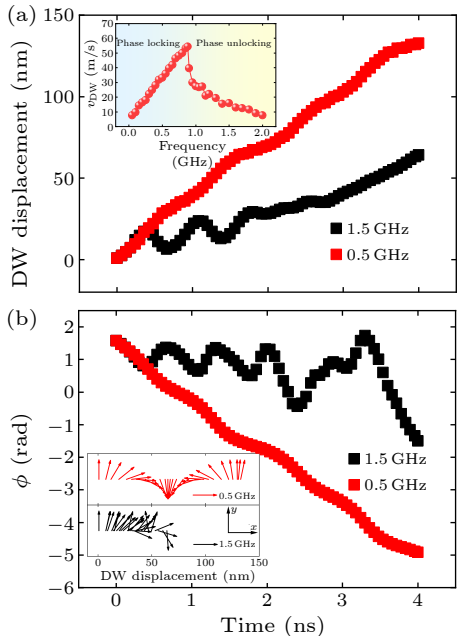

Fig. 4. (a) Displacement of the DW driven by the 30-degree SAW at the frequencies of 0.5 and 1.5 GHz (inset: variation of DW velocity as a function of the frequency of the 30-degree SAW). (b) Variation of the azimuthal angle at the frequencies of 0.5 and 1.5 GHz (inset: variation of the orientation of the magnetization in the DW center with the DW motion).

demonstrate that this phenomenon originates from unstable solutions of the DW nonlinear dynamic equations.

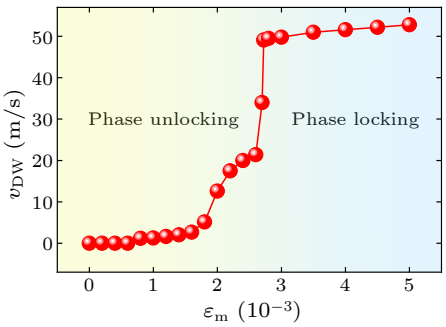

Fig. 5. DW velocity as a function of the strain amplitude for the 30-degree SAW at a frequency of 0.8 GHz.

The amplitude of strain (ε_m) also influences the DW velocity in a similar way (Fig. 5). In the simulation, above a threshold ε_m ($\varepsilon_{m,th}$) around 0.0027, the DW velocity becomes almost stable, and below it, the DW velocity decreases with the reducing ε_m. We will show that the appearance of this threshold ε_m is also relevant to the transition between the phase-locking and phase-unlocking magnetization precession.

The simulated DW motion with phase-locking characteristics can be derived by using the collective coordinate method (CCM). We started with the Lagrangian density function,[21]

$$\begin{aligned} L_{dens} &= E_{dens} + \frac{M_s}{\gamma}\dot{\phi}\cos\theta \\ &= \frac{A_{ex}}{\Delta^2}\sin^2\theta + K_u\sin^2\theta + \frac{\mu_0}{2}M_s(N_x\sin^2\theta\cos^2\phi \\ &\quad + N_y\sin^2\theta\sin^2\phi + N_z\cos^2\phi) + b_1\varepsilon_{xx}\cos^2\phi\sin^2\theta \\ &\quad + 2b_2\varepsilon_{xy}\sin\phi\cos\phi\sin^2\theta + \frac{M_s}{\gamma}\dot{\phi}\cos\theta. \end{aligned} \tag{4}$$

Here θ, ϕ, and Δ are the polar angle, azimuthal angle, and the DW width, and θ satisfies $\tan\frac{\theta}{2} = \exp[\frac{x-q}{\Delta}]$ with q as the DW central position. N_x, N_y, and N_z are the demagnetizing factors in the x, y, and z directions, respectively. $\frac{M_s}{\gamma}\dot{\phi}\cos\theta$ is the precession term. For simplicity, we neglect the spatial dependence of strain as the SAW wavelength is approximately 4 μm, which is much longer than the DW width, i.e., $\varepsilon_{xx} = \varepsilon_m\sin(\omega t)$, $\varepsilon_{xy} = \frac{1}{2}\varepsilon_m\sin(\omega t + \pi/2)$, and our simulation confirms that neglecting the spatial variation of strain components has a negligible impact on DW dynamics. Additionally, we did not consider the influence of the variation of strain on the DW width, since we verified that the oscillation of DW width under strain of the 30-degree SAW does not have a considerable impact on the DW velocity (S3 in the SM).

The Rayleigh dissipation density function is

$$F_{dens} = \frac{\alpha M_s}{2\gamma}\left(\frac{d\boldsymbol{m}}{dt}\right)^2 = \frac{\alpha M_s}{2\gamma}\left(\frac{\dot{q}^2}{\Delta^2} + \dot{\phi}^2\right)\sin^2\theta. \tag{5}$$

The spatial integral of L_{dens} and F_{dens} yields the Lagrangian L and Rayleigh dissipation function F. Based on the Euler–Lagrange–Rayleigh equation: $\frac{\partial L}{\partial q_i} - \frac{d}{dt}(\frac{\partial L}{\partial \dot{q}_i}) + \frac{\partial F}{\partial \dot{q}_i} = 0$ with $q_i = q$, ϕ, we deduced the Thiele equations,

$$\dot{\phi} + \frac{\alpha\dot{q}}{\Delta} = 0, \tag{6}$$

$$\begin{aligned} \frac{\dot{q}}{\Delta} - \alpha\dot{\phi} &= \frac{1}{2}\mu_0\gamma M_s(N_y - N_x)\sin 2\phi - \frac{\varepsilon_m\gamma b_1}{M_s}\sin(\omega t)\sin 2\phi \\ &\quad + \frac{\varepsilon_m\gamma b_2}{M_s}\cos(\omega t)\cos 2\phi. \end{aligned} \tag{7}$$

The initial DW width extracted from the simulation is $\Delta = 5.9$ nm. According to the method in Ref. [22], for a square film system, $N_x \approx N_y$. Therefore, in the following analysis, the contribution of the demagnetization term is neglected.

The crucial role of the SAW spin in driving DWs lies in two magnetoelastic terms with a $\pi/2$ phase difference on the right side of Eq. (7). By defining $b_1 = b_2 = b$, and substituting Eq. (6) into Eq. (7), we converted the dynamics equation of ϕ to

$$\left(\alpha + \frac{1}{\alpha}\right)\dot{\phi} = -\frac{\varepsilon_m\gamma b}{M_s}\cos(\omega t + 2\phi). \tag{8}$$

Both of the numerical solutions of Eq. (8) and the simulation illustrate an approximately linear variation of ϕ at lower frequencies, which, as indicated in Eq.(6), should lead to a constant DW velocity. On the other hand, the linear variation of ϕ will further give rise to a constant $\omega t + 2\phi$ in Eq.(8), that is, C remains constant. Therefore, $\dot{\phi} = -\frac{\omega}{2}$, demonstrating the phase-locking magnetization precession in a moving DW at the velocity

$$\dot{q} = \frac{\omega\Delta}{2\alpha} = \frac{\Delta\varepsilon_m\gamma b}{(\alpha^2+1)M_s}\cos(C). \tag{9}$$

The threshold values of frequency and ε_m in Figs. 4 and 5 originate from the issue that $|\cos(C)|$ should not exceed 1. Based on Eq. (9), the linear increase of the DW velocity cannot be maintained when the frequency exceeds the threshold

$$\omega_{th} = \frac{2\alpha\varepsilon_m\gamma|b|}{(\alpha^2+1)M_s}, \tag{10}$$

or when ε_m is smaller than the critical value

$$\varepsilon_{m,th} = \frac{(\alpha^2+1)M_s}{2\alpha\gamma|b|}\omega, \tag{11}$$

and the magnetization precession in DW will become phase-unlocking. This gives rise to the oscillation of the DW displacement and the gradual reduction of the DW velocity.

According to Eqs. (8) and (10), the temporal variation of phase C satisfies the following equation:

$$\frac{dC}{dt} = \omega + \omega_{th}\cos(C). \tag{12}$$

During the phase unlocking, the period of C can be characterized as[23]

$$T = \int_0^{2\pi}\frac{dt}{dC}dC = \int_0^{2\pi}\frac{dC}{\omega + \omega_{th}\cos(C)} = \frac{2\pi}{\sqrt{\omega^2 - \omega_{th}^2}}, \tag{13}$$

which corresponds to the time required for changing C by 2π. Since $\phi = \frac{1}{2}(C - \omega t)$, this indicates that when the frequency exceeds the threshold, the magnetization azimuth angle will superimpose a periodic variation on its linear progression. According to Eq. (6), the velocity for the DW displacement is proportional to the variation speed of ϕ.

This explains the oscillatory nature of the DW displacement observed in Fig. 4 under the 1.5 GHz SAW frequency, which is higher than the $f_{\rm th}$. Very interestingly, this phase-unlocking DW dynamics appears to be well analogous to the phase-unlocking lighting of fireflies proposed by Ermentrout and Rinzel in 1984.[23]

The estimation of the limit of angular frequency is in good agreement with the simulation: Under the strain amplitude of 0.003, the theoretical threshold angular frequency is $\omega_{\rm th} = 2\pi \times 1.26\,{\rm GHz}$, close to the simulated $\omega_{\rm th}$ ($2\pi \times 0.88\,{\rm GHz}$). On the other hand, under the acoustic wave frequency of 0.8 GHz, the theoretical $\varepsilon_{\rm m,th}$ is 0.002, which is also close to the simulated value $\varepsilon_{\rm m,th} = 0.0027$. The discrepancy between the theoretical model results and the simulation may stem from the assumed constant DW width in the CCM. In principle, when the strain exceeds the saturation value, the DW velocity would stabilize. However, the simulation shows a slight increase in the DW velocity when the strain exceeds 0.0027. This is mainly because of the modulation of the DW width under SAW (S3 in the SM).

The transition between phase-locking and phase-unlocking magnetization precession can also be understood based on the variation of the angle ζ in Fig. 2(a). During the phase-locking process, C represents a constant for the magnetization at the DW center, and the angle ζ decreases with increasing frequency or decreasing strain amplitude. At the threshold frequency or strain amplitude, $C = \pi$, and the average $\boldsymbol{H}_{\rm me}$ becomes strictly perpendicular to the magnetization. Under this situation, the strength of the field for driving the magnetization precession reaches its maximum value, and the DW moves at its highest velocity.

For comparison, we also conducted a brief discussion on the interaction between DWs and pure Rayleigh or SH SAWs (S4 in the SM). In the Thiele equation, either type of SAW induces equally strong clockwise and counterclockwise precession tendencies in the magnetization of DW center. As a result, the driving forces for both forward and backward DW motion remain identical, making unidirectional DW motion unachievable.

In conclusion, we have demonstrated that SAWs maintain a uniform constant spin angular momentum as they propagate at a 30-degree angle relative to the x-axis crystal orientation of 128° Y-$LiNbO_3$. We have confirmed that the out-of-plane acoustic spin offers the FL and DL torques that have the same expression as that of STT. These torques induce DW motion at velocities exceeding 50 m/s, significantly surpassing the velocities achieved with conventional Rayleigh and SH SAWs. In addition, the DW motion undergoes a transition between phase-locking and phase-unlocking regimes at critical values of SAW frequency or strain amplitude. These findings present a novel mechanism for achieving high-speed DW motion by utilizing the acoustic spin, paving the way for energy-efficient spintronic device applications.

Acknowledgements. This work was supported by the National Key Research and Development Program of China (Grant No. 2022YFE0103300), the open research fund of Songshan Lake Materials Laboratory (Grant No. 2023SLABFN26), and the Natural Science Foundation of Hubei Province (Grant No. 2022CFA088).

References

[1] Huang M X, Hu W B, and Bai F M 2024 *Acta Phys. Sin.* **73** 158501 (in Chinese)
[2] Puebla J, Hwang Y, Maekawa S, and Otani Y 2022 *Appl. Phys. Lett.* **120** 220502
[3] Vlasov V, Golov A, Kotov L, Shcheglov V, Lomonosov A, and Temnov V 2022 *Acoust. Phys.* **68** 18
[4] Yang W G and Schmidt H 2021 *Appl. Phys. Rev.* **8** 021304
[5] Kuess M, Albrecht M, and Weiler M 2022 *Front. Phys.* **10** 981257
[6] Saiz P G, De Luis R F, Lasheras A, Arriortua M I, and Lopes A C 2022 *Acs Sens.* **7** 1248
[7] Weiler M, Dreher L, Heeg C, Huebl H, Gross R, Brandt M S, and Goennenwein S T B 2011 *Phys. Rev. Lett.* **106** 117601
[8] Dreher L, Weiler M, Pernpeintner M, Huebl H, Gross R, Brandt M S, and Goennenwein S T B 2012 *Phys. Rev. B* **86** 134415
[9] Weiler M, Huebl H, Goerg F, Czeschka F D, Gross R, and Goennenwein S T B 2012 *Phys. Rev. Lett.* **108** 176601
[10] Chen R, Chen C, Han L, Liu P, Su R, Zhu W, Zhou Y, Pan F, and Song C 2023 *Nat. Commun.* **14** 4427
[11] Edrington W, Singh U, Dominguez M A, Alexander J R, Nepal R, and Adenwalla S 2018 *Appl. Phys. Lett.* **112** 052402
[12] Shuai J, Lopez-Diaz L, Cunningham J E, and Moore T A 2023 *Phys. Rev. B* **108** 104420
[13] Yang Y, Zhao L, Yi D, Xu T, Chai Y H, Zhang C Y, Jiang D S, Ji Y H, Hou D Z, Jiang W J, Tang J S, Yu P, Wu H Q, and Nan T X 2024 *Nat. Commun.* **15** 1018
[14] Yokouchi T, Sugimoto S, Rana B, Seki S, Ogawa N, Kasai S, and Otani Y 2020 *Nat. Nanotechnol.* **15** 361
[15] Long Y, Ren J, and Chen H 2018 *Proc. Natl. Acad. Sci.* **115** 9951
[16] Long Y, Zhang D, Yang C, Ge J, Chen H, and Ren J 2020 *Nat. Commun.* **11** 4716
[17] Shi C, Zhao R, Long Y, Yang S, Wang Y, Chen H, Ren J, and Zhang X 2019 *Nat. Sci. Rev.* **6** 707
[18] Liao L Y, Chen F, Puebla J, Kishine J, Kondou K, Luo W, Zhao D G, Zhang Y, Ba Y, and Otani Y 2024 *Sci. Adv.* **10** eado2504
[19] Garanin D and Chudnovsky E 2015 *Phys. Rev. B* **92** 024421
[20] Vanderveken F, Mulkers J, Leliaert J, Van Waeyenberge B, Sorée B, Zografos O, Ciubotaru F, and Adelmann C 2021 *Open Res. Europe* **1** 35
[21] Vandermeulen J, Nasseri S, Van de Wiele B, Durin G, Van Waeyenberge B, and Dupré L 2018 *J. Magn. Magn. Mater.* **449** 337
[22] Aharoni A 1998 *J. Appl. Phys.* **83** 3432
[23] Strogatz S H 2018 *Nonlinear dynamics and chaos: with applications to physics, biology, chemistry, and engineering* (CRC Press)